Imaging Anomalous Nematic Order and Strain in Optimally Doped $BaFe_2(As,P)_2$

Eric Thewalt,[1,2] Ian M. Hayes,[1,2] James P. Hinton,[1,2] Arielle Little,[1,2] Shreyas Patankar,[1,2] Liang Wu,[1,2] Toni Helm,[1,2] Camelia V. Stan,[3] Nobumichi Tamura,[3] James G. Analytis,[1,2] and Joseph Orenstein[1,2]
[1]*Department of Physics, University of California, Berkeley, California 94720, USA*
[2]*Materials Science Division, Lawrence Berkeley National Laboratory, Berkeley, California 94720, USA*
[3]*Advanced Light Source, Lawrence Berkeley National Laboratory, Berkeley, California 94720, USA*

(Received 14 September 2017; published 9 July 2018)

We present the strain and temperature dependence of an anomalous nematic phase in optimally doped $BaFe_2(As,P)_2$. Polarized ultrafast optical measurements reveal broken fourfold rotational symmetry in a temperature range above T_c in which bulk probes do not detect a phase transition. Using ultrafast microscopy, we find that the magnitude and sign of this nematicity vary on a 50–100 μm length scale, and the temperature at which it onsets ranges from 40 K near a domain boundary to 60 K deep within a domain. Scanning Laue microdiffraction maps of local strain at room temperature indicate that the nematic order appears most strongly in regions of weak, isotropic strain. These results indicate that nematic order arises in a genuine phase transition rather than by enhancement of local anisotropy by a strong nematic susceptibility. We interpret our results in the context of a proposed surface nematic phase.

DOI: 10.1103/PhysRevLett.121.027001

Iron-based superconductors [1–3] have been the subject of significant interest largely as a result of evidence for quantum criticality [4–12] accompanied by divergent nematic susceptibility [13–17] in the vicinity of optimal doping. These phenomena have been associated with an enhancement of the superconducting critical temperature T_c [18–20].

Evidence for a quantum critical point (QCP) near optimal doping is particularly strong in $BaFe_2(As_{1-x}P_x)_2$, or P:Ba122, an isoelectronically doped superconductor. At high temperature, this material has a tetragonal crystal structure, shown in Fig. 1(a), consisting of layers of Fe ions arranged in a square lattice with a pnictogen ion alternating above and below the center of each plaquette and Ba ions between the layers. The parent compound $BaFe_2As_2$ undergoes simultaneous tetragonal-to-orthorhombic and Néel spin-density-wave (SDW) transitions at $T_N \approx 150$ K [21], breaking fourfold rotational (C_4) symmetry. Substitution of As by P [22] and c-axis compression [23] each suppress T_N by reducing the average height of pnictogen ions and widening the Fe $3d$ bands, which destabilizes the SDW order [24]. Bulk probes, including neutron and x-ray scattering, transport, NMR [25], and specific heat [9], indicate that the SDW phase onsets above T_c for a P concentration up to, but not above, $x = 0.29$, just below optimal doping ($x = 0.3$).

Despite the evidence from these bulk probes, persistent hints that C_4 symmetry is broken in samples with $x > 0.3$ suggest that there is more to the story. Angle-resolved photoemission (ARPES) [26,27] and torque magnetometry [28] studies have found evidence of broken C_4 symmetry above the dome of superconductivity persisting above optimal doping in P:Ba122, and optical data suggest similar behavior in $Ba(Fe,Co)_2As_2$ [29].

The simplest explanation for this apparent discrepancy is that typical samples are under strain. This strain can either be frozen in during crystal growth, which we call intrinsic strain, or caused by the crystal mounting and cooling processes, which we call extrinsic strain. Such strain, when coupled with a diverging nematic susceptibility near the QCP, would induce nematic order that would strengthen rapidly but smoothly with a decreasing temperature. However, the measurements of nematicity at $x > 0.3$ indicate that it tends to have an abrupt onset [26,27,29], and our results corroborate this observation.

In this Letter, we present a study of nematicity in optimally doped P:Ba122, with the aim of resolving the apparent contradiction between implications from different experiments. We map a single region of a P:Ba122 crystal with two local probes of broken C_4: time-resolved optical pump-probe reflectance, or photomodulation, which enhances weak structure in the reflectance R [30], and scanning Laue microdiffraction [31], which allows us to explore the link between local strain and the onset and strength of nematicity. Our photomodulation measurements reveal nematic order above T_c, with the magnitude, sign, and onset temperature varying on a length scale of 50–100 μm.

Contrary to expectation, we find that the nematic order observed via photomodulation is strongest in regions where uniaxial strain and transverse dilation are weakest. However, the boundaries of domains of nematic order coincide with sharp features in local strain. This suggests that the nematic order develops in a genuine phase transition rather than as a result of local anisotropy amplified by a strong nematic susceptibility. Our results are consistent with a surface nematic phase, as has been suggested by calculations

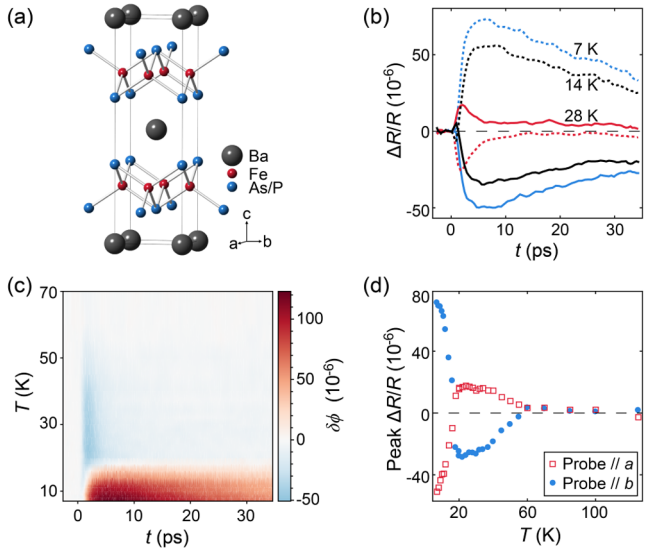

FIG. 1. Crystal structure of P:Ba122 and photomodulation results at optimal doping. (a) Crystal structure of P:Ba122. (b) Pump-probe response $\Delta R/R$ as a function of time at a fixed position, with probe polarization parallel to the Fe-Fe directions a (solid lines) and b (dotted lines). Red, black, and blue traces correspond to $T = 28$, 14, and 7 K, respectively, spanning the apparent superconducting transition temperature. (c) Time and temperature dependence of the C_4-odd photomodulation response $\delta\phi \equiv (\Delta R_b - \Delta R_a)/R$. (d) Temperature dependence of the maximum-amplitude value of $\Delta R(t)/R$ for probe polarization along a (red) and b (blue), illustrating near-perfect antisymmetry under a $\pi/2$ rotation of the probe polarization, abrupt onset of broken C_4 symmetry, and competition between superconductivity and nematic order.

incorporating interlayer hopping [32]. The existence of such a phase would relieve the tension between results from bulk and surface probes.

Measurements of photomodulated reflectance ΔR were performed using linearly polarized, 100-fs-duration pulses from a mode-locked Ti:sapphire laser at 80 MHz repetition rate, 800 nm center wavelength, and $\sim 5\ \mu\mathrm{J/cm^2}$ fluence. Our initial measurements showed a strong dependence of the amplitude and sign of ΔR on the position of the pump-probe focus on the sample surface. As a result, local characterization of the time and temperature dependence of ΔR required an accurate stabilization of the position of the laser focus relative to the sample during cooling. This was achieved by registering the sample to an optical landmark on its mount using a high-resolution video feed, enabling us to fix the focal position with a precision of 5 μm. Figure 1(b) shows examples of pump-probe traces measured at a fixed position on a sample with $x = 0.31$ at three temperatures spanning the apparent superconducting transition, with the probe polarized along the orthogonal Fe-Fe directions, which we (arbitrarily) label a and b (solid and dotted lines, respectively). (The stated temperatures are nominal; the actual crystal temperature at the laser focus is higher as a result of laser heating. We studied the apparent superconducting transition temperature as a function of laser fluence and confirmed that T_c approaches 31 K at low fluence; the results are shown in Ref. [33].)

The photomodulation data show striking evidence of broken C_4 symmetry. In the presence of C_4 symmetry, ΔR would be independent of the polarization of the probe electric field; that is, $\Delta R_a = \Delta R_b$. Instead, the pump-probe response is approximately equal and opposite along orthogonal Fe-Fe directions, i.e., $\Delta R_a \approx -\Delta R_b$. In the subsequent discussion, we consider the strength of the C_4-odd component of the photomodulation response, $(\Delta R_b - \Delta R_a)/R \equiv \delta\phi$, to be a proxy for nematic order (see [34] for details).

The full time and temperature dependence of $\delta\phi$ is shown in Fig. 1(c). There are two distinct forms of pump-probe response: Above the superconducting transition, the response is short-lived and $\delta\phi$ is negative; well below T_c, the response is long-lived and $\delta\phi$ is positive. Near the transition, both forms are apparent. To better illustrate the singular features of the temperature dependence, we plot in Fig. 1(d) the maximum-amplitude value of $\Delta R(t)/R$ as a function of temperature for a and b probe polarizations. With decreasing temperature, ΔR first appears abruptly above the noise at $\sim$60 K. Upon further cooling, the sign of ΔR changes abruptly near T_c, and at low temperature the sign is reversed relative to the normal state.

The change in sign and relaxation rate at T_c can be understood on the basis of competition between the nematic order parameter ϕ and the superconducting order parameter ψ. For $T > T_c$, the pump pulse weakens the nematic order, which then returns rapidly to its equilibrium value. However, for $T < T_c$, the pump also suppresses ψ, and, since the timescale of this suppression is longer than that of the nematic order, a quasiequilibrium results in which ϕ is enhanced due to the mutual repulsion of ϕ and ψ. The enhancement of ϕ persists until ψ returns to its equilibrium amplitude. For a detailed discussion of this model, refer to Ref. [35].

The observation of broken C_4 at a fixed location on the sample surface strongly suggests domain formation as the origin of the position dependence described above. To test this hypothesis, we mapped the variation of $\delta\phi$ on the sample surface. These maps were obtained by mounting samples onto an xyz piezo stage and scanning the sample with respect to an 8 μm diameter focus of overlapping pump and probe beams. The P:Ba122 crystal was mounted on a Cu plate, providing a net 0.2% compressive strain on the base of the sample via thermal contraction.

A map of local nematicity obtained by spatially resolved photomodulation is shown in Fig. 2(a). The color of each square encodes the maximum-amplitude value $\delta\phi_M$ of $[\Delta R_b(t) - \Delta R_a(t)]/R$, that is, of the difference between ΔR measured along the two principal axes. Domain boundaries separating regions of broken C_4 symmetry with

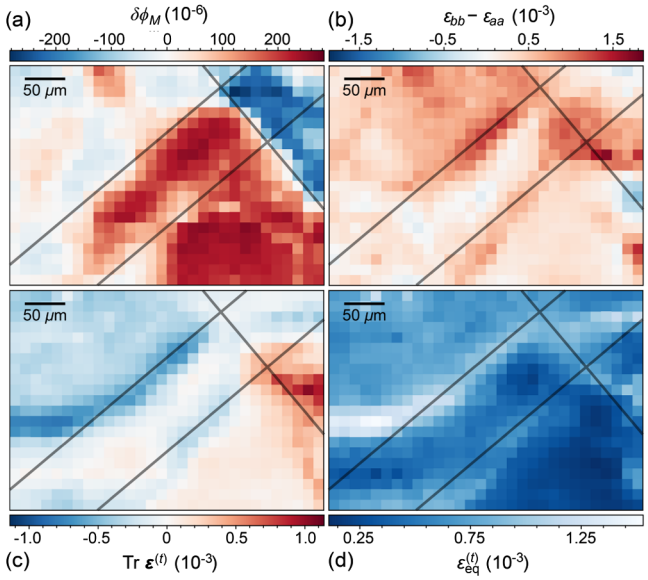

FIG. 2. Spatial variation (13 μm resolution) of optical anisotropy (a) and ab-plane strain (b)–(d) on a 390×260 μm region of an optimally doped P:Ba122 crystal mounted on Cu. (a) Photomodulation proxy for nematic order, $\delta\phi_M$. (b) Transverse strain anisotropy $\varepsilon_{bb} - \varepsilon_{aa}$ in the Fe-Fe basis. (c) Transverse unit cell dilation $\mathrm{Tr}\boldsymbol{\varepsilon}^{(t)}$. (d) Transverse equivalent strain $\varepsilon_{\mathrm{eq}}^{(t)} = (2\varepsilon_{ij}^{(t)}\varepsilon_{ij}^{(t)}/3)^{1/2}$. Superimposed lines are parallel to the Fe-Fe directions and are located at the same positions in each image to facilitate a visual comparison of features. Optical data were collected at $T = 5$ K, strain data at room temperature.

orthogonal nematic order are readily apparent. We note that the typical domain size of $\sim$100 μm is large compared to the $\sim$10 μm structural domains that have been imaged using polarized light below the structural transition in underdoped P:Ba122 [36–38] and that 100 μm is the approximate size of crystals used in the previously cited torque magnetometry experiments that suggested a broad nematic phase above the superconducting dome [28].

The spatial patterns of positive and negative $\delta\phi_M$ do not change with repeated heating and cooling of the sample, suggesting that the magnitude and sign of the nematic order are determined by some local quantity. A local strain field, perhaps frozen into the crystal during growth, is a natural candidate; a difference between the strains along orthogonal Fe-Fe directions would couple directly to C_4-breaking order [39]. Another potential contributing factor is local in-plane compression of the unit cell [40], which would increase the pnictogen height and the Fe—As—Fe bond angle, counteracting the effect of P doping [24] and driving the crystal back toward the underdoped SDW phase.

In order to explore the link between local strain and the onset of nematic order, we used scanning Laue (i.e., polychromatic) microdiffraction to map the local strain at room temperature in the same region of the sample that was imaged using photomodulation (see [41] for details on the region-alignment procedure). A full diffraction pattern was collected at each position and used, along with the known lattice parameters, to extract the deviatoric (i.e., traceless) strain tensor $\boldsymbol{\varepsilon}$, which describes the local deformation of the unit cell. In a given basis, the diagonal components ε_{aa}, ε_{bb}, and ε_{cc} of the strain tensor correspond to expansion (or compression, for negative values) along the corresponding direction, while the off-diagonal components ε_{ab}, ε_{bc}, and ε_{ca} correspond to pure shear. Since we are primarily concerned with strain in the Fe-As layers, we focus on the ab subsector of $\boldsymbol{\varepsilon}$, which we denote by $\boldsymbol{\varepsilon}^{(t)}$. The dilation of the ab-plane unit cell is given by $\mathrm{Tr}\boldsymbol{\varepsilon}^{(t)} = \varepsilon_{aa} + \varepsilon_{bb}$; compression corresponds to negative values.

Figure 2 illustrates the relationship between the previously discussed map of low-temperature optical anisotropy in Fig. 2(a) and the spatial variation of the strain tensor in Figs. 2(b)–2(d). The superimposed lines, oriented with the Fe-Fe directions a and b, are positioned identically on each image. Figure 2(b) shows the strain anisotropy in the Fe-Fe basis, $\varepsilon_{bb} - \varepsilon_{aa}$, in the same region of the crystal. Contrary to what would be expected if the nematic order were the result of a local strain bias, the changes in sign of $\delta\phi_M$ and the Fe-Fe strain anisotropy do not coincide. Furthermore, the Fe-Fe strain anisotropy is small in magnitude in most of the region where the nematic photomodulation response is strongest. Figure 2(c) shows the transverse unit-cell dilation $\mathrm{Tr}\boldsymbol{\varepsilon}^{(t)}$, which is small and mostly positive in the large region corresponding to large positive $\delta\phi_M$, contradicting the prediction that negative $\mathrm{Tr}\boldsymbol{\varepsilon}^{(t)}$ would drive the system toward the C_4-breaking SDW phase. Finally, Fig. 2(d) shows the equivalent strain $\varepsilon_{\mathrm{eq}}^{(t)} = (2\varepsilon_{ij}^{(t)}\varepsilon_{ij}^{(t)}/3)^{1/2}$, a measure of the total strain. Although the nematic order and the strain anisotropy are not strongly correlated, the edges of the nematic domains are coincident with strain features, in particular, with local maxima in the equivalent strain and with extrema in $\mathrm{Tr}\boldsymbol{\varepsilon}^{(t)}$. (We note that the observed strain variations are likely intrinsic rather than extrinsic, as we observed similar variations in an optimally doped crystal mounted strain-free; see [42] for details.)

Taken together, these results strongly suggest that local strain is not the driver, via divergent susceptibility, of the nematicity we observe—in fact, strong strain anisotropy (and strong strain, in general) appears to suppress the electronic nematicity.

In order to further study the effect of extrinsic uniaxial strain, we also performed ultrafast microscopy on an optimally doped sample mounted on a piezoelectric stack. On cooling, the piezo provides a tensile uniaxial strain by thermally contracting by 0.1% (similar to optimally doped P:Ba122) along one lateral dimension while expanding by 0.1% along the other. The crystal's Fe-Fe directions were aligned with these principal piezo axes. The resulting image of $\delta\phi_M$ is shown in Fig. 3(a). The domain population of the uniaxially strained crystal differs significantly from that of the Cu-mounted sample, as is evident in Fig. 3(b),

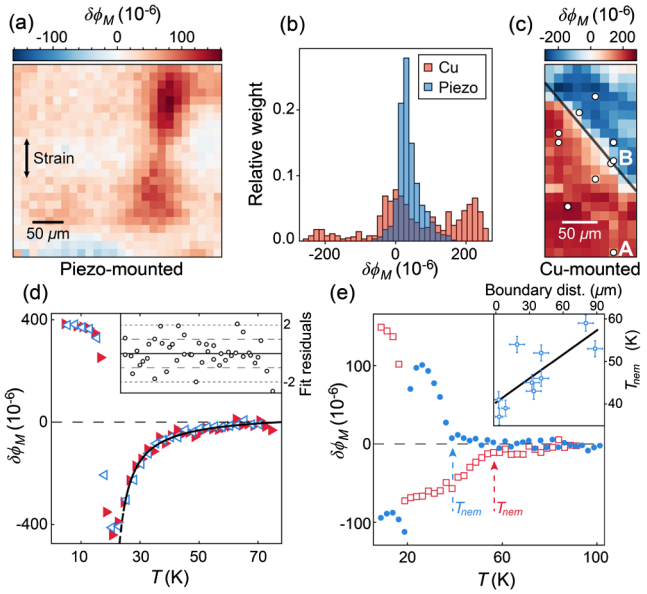

FIG. 3. Comparison of spatial variation (13 μm resolution) and temperature dependence of nematic order for piezo-mounted (uniaxially strained) and Cu-mounted (biaxially strained) crystals. (a) Spatial variation of photomodulation proxy for nematic order, $\delta\phi_M$, on the piezo-mounted crystal, which is uniaxially strained as indicated. (b) Histograms showing the distribution of $\delta\phi_M$ for both crystals. (c) Spatial variation of $\delta\phi_M$ on the Cu-mounted crystal, with open circles indicating positions at which temperature dependence data were collected and a black line marking a region of null $\Delta R/R$ response separating regions of opposite nematic sign. (d) Temperature dependence of $\delta\phi_M$ for the piezo-mounted crystal while warming (right-pointed triangles) and cooling (left-pointed triangles). The black line is a Curie-Weiss fit with $T_{\mathrm{CW}} = 19$ K (solid on the fitted domain, dashed at lower temperatures). Inset: Standardized fit residuals. (e) Temperature dependence of $\delta\phi_M$ for the Cu-mounted crystal far from the boundary at the point marked A (open squares) and near the boundary at the point marked B (circles). Apparent nematic transition temperatures are indicated. Inset: Scatter plot of the nematic transition temperature as a function of distance from the domain boundary indicated by the black line in (c); correlation is positive with p value $< 10^{-2}$.

which compares histograms of $\delta\phi_M$ in both samples. The uniaxial strain appears to bias the domain population, shifting the central Cu peak while suppressing the large-amplitude nematic response. Thus, while intrinsic strain defies expectation, extrinsic strain biases the electronic nematicity in the expected manner.

In addition to pump-probe microscopy, we measured the temperature dependence of $\delta\phi_M$ on both crystals, including at multiple points on the Cu-mounted sample. These points are indicated by white circles in Fig. 3(c), and the points marked A and B correspond, respectively, to the red and blue $\delta\phi_M(T)$ markers in Fig. 3(e), where $\delta\phi_M$ is plotted as a function of temperature.

The onset of the nematic optical response in the Cu-mounted crystal is abrupt at each position and is manifestly distinct from a smooth Curie-Weiss behavior. The onset temperature varies between approximately 40 and 60 K and is positively correlated (p value $< 10^{-2}$) with distance from the line of null nematic response, as illustrated in Fig. 3(e). This range of onset temperatures is consistent with ARPES measurements [27] but is lower than the 100 K onset observed via torque magnetometry [28].

In contrast to the Cu-mounted sample, the temperature dependence of $\delta\phi_M$ on the piezo-mounted crystal is well described by a Curie-Weiss form with transition temperature $T_{\mathrm{CW}} = 19$ K. The fit (black line, solid on fitted region) and data are shown in Fig. 3(d), with the standardized fit residuals in the inset. In the presence of strong, uniform uniaxial strain, therefore, we observe a nematic onset that is consistent with the picture of a divergent nematic susceptibility, which makes the sharpness of the nematic onset in the Cu-mounted sample all the more notable. We do not observe any hysteretic difference between the data collected with increasing temperature (right-pointed markers) and with decreasing temperature (left-pointed markers).

The strong correlation between the nematic onset temperature and distance from the boundary between the positive and negative domains suggests that we may be observing a nucleation phenomenon, where the nematic domains arise deterministically at some distant crystalline features and then spread as the temperature decreases until they reach the high-equivalent-strain boundaries indicated in Fig. 2(d). This picture is particularly compelling in light of recent work incorporating hopping between Fe-As layers, which has shown that interlayer hopping can produce a surface nematic phase that onsets at significantly higher temperatures than in the bulk [32]. A surface phase, which could also arise due to the stabilization of fluctuating order by soft surface phonons [43], would be more susceptible to confinement by boundaries of strain due to the reduced dimensionality and volume of the required region of contiguous deformation and could be disfavored under transverse compression due to buckling-induced disorder. In addition, this model is consistent both with surface measurements that indicate a genuine nematic phase ([26,27,29], and this work) and with bulk measurements that show no evidence of a phase transition [9,22,25]. An important open question that remains is what mechanism deterministically selects the sign of the nematic order at a given point on the crystal surface.

In conclusion, photomodulation measurements reveal that optimally doped $BaFe_2(As,P)_2$ has a C_4-breaking phase well above T_c that varies strongly in magnitude, sign, and onset temperature at length scales of $50-100$ μm. Scanning Laue microdiffraction measurements show that the local strain anisotropy and local transverse compression of the unit cell, which are both expected to favor nematic order, are anticorrelated with the observed optical nematicity. These results imply that the optical nematicity in the

biaxially strained crystal corresponds to a genuine nematic phase transition rather than the amplification of local anisotropy by an enhanced nematic susceptibility. We interpret this phase as a surface phenomenon [32] that nucleates well above T_c and spreads until it reaches boundaries where the crystal is highly strained. A surface nematic phase with large domains reconciles ARPES [26,27], optical [29], and torque magnetometry [28] measurements showing nematic order at optimal doping with bulk measurements [9,22,25] that do not show a phase transition. In general, phase diagrams of two-dimensional materials may differ significantly from those based on bulk measurements of the same compound.

We thank E. Angelino, R. Fernandes, I. Fisher, F. Flicker, A. Koshelev, K. Song, and N. Yao for helpful discussions. Measurements and modeling were performed at the Lawrence Berkeley National Laboratory in the Quantum Materials program supported by the Director, Office of Science, Office of Basic Energy Sciences, Materials Sciences and Engineering Division, of the U.S. Department of Energy under Contract No. DE-AC02-05CH11231. Synthesis of P:Ba122 was supported by Laboratory Directed Research and Development Program of Lawrence Berkeley National Laboratory under Contract No. DE-AC02-05CH11231. J. O., L. W., and A. L. received support for performing and analyzing optical measurements from the Gordon and Betty Moore Foundation's EPiQS Initiative through Grant No. GBMF4537 to J. O. at UC Berkeley. Material synthesis and characterization was supported by the Gordon and Betty Moore Foundation's EPiQS Initiative Grant No. GBMF4374 to J. A. at UC Berkeley. Laue microdiffraction measurements were carried out at beam line 12.3.2 at the Advanced Light Source, which is a Department of Energy User Facility under Contract No. DE-AC02-05CH11231.

[1] Y. Kamihara, T. Watanabe, M. Hirano, and H. Hosono, J. Am. Chem. Soc. **130**, 3296 (2008).
[2] H. Takahashi, K. Igawa, K. Arii, Y. Kamihara, M. Hirano, and H. Hosono, Nature (London) **453**, 376 (2008).
[3] M. Rotter, M. Tegel, and D. Johrendt, Phys. Rev. Lett. **101**, 107006 (2008).
[4] H. Shishido *et al.*, Phys. Rev. Lett. **104**, 057008 (2010).
[5] S. Kasahara *et al.*, Phys. Rev. B **81**, 184519 (2010).
[6] Y. Nakai, T. Iye, S. Kitagawa, K. Ishida, H. Ikeda, S. Kasahara, H. Shishido, T. Shibauchi, Y. Matsuda, and T. Terashima, Phys. Rev. Lett. **105**, 107003 (2010).
[7] E. Abrahams and Q. Si, J. Phys. Condens. Matter **23**, 223201 (2011).
[8] K. Hashimoto *et al.*, Science **336**, 1554 (2012).
[9] P. Walmsley *et al.*, Phys. Rev. Lett. **110**, 257002 (2013).
[10] J. G. Analytis, H. H. Kuo, R. D. McDonald, M. Wartenbe, P. M. C. Rourke, N. E. Hussey, and I. R. Fisher, Nat. Phys. **10**, 194 (2014).
[11] T. Shibauchi, A. Carrington, and Y. Matsuda, Annu. Rev. Condens. Matter Phys. **5**, 113 (2014).
[12] H.-H. Kuo, J.-H. Chu, J. C. Palmstrom, S. A. Kivelson, and I. R. Fisher, Science **352**, 958 (2016).
[13] L. W. Harriger, H. Q. Luo, M. S. Liu, C. Frost, J. P. Hu, M. R. Norman, and P. Dai, Phys. Rev. B **84**, 054544 (2011).
[14] M. Yi *et al.*, Proc. Natl. Acad. Sci. U.S.A. **108**, 6878 (2011).
[15] J.-H. Chu, H.-H. Kuo, J. G. Analytis, and I. R. Fisher, Science **337**, 710 (2012).
[16] A. E. Böhmer, P. Burger, F. Hardy, T. Wolf, P. Schweiss, R. Fromknecht, M. Reinecker, W. Schranz, and C. Meingast, Phys. Rev. Lett. **112**, 047001 (2014).
[17] R. M. Fernandes, A. V. Chubukov, and J. Schmalian, Nat. Phys. **10**, 97 (2014).
[18] M. A. Metlitski, D. F. Mross, S. Sachdev, and T. Senthil, Phys. Rev. B **91**, 115111 (2015).
[19] S. Lederer, Y. Schattner, E. Berg, and S. A. Kivelson, Phys. Rev. Lett. **114**, 097001 (2015).
[20] T. A. Maier and D. J. Scalapino, Phys. Rev. B **90**, 174510 (2014).
[21] Q. Si, R. Yu, and E. Abrahams, Nat. Rev. Mater. **1**, 16017 (2016).
[22] J. M. Allred *et al.*, Phys. Rev. B **90**, 104513 (2014).
[23] W. J. Duncan, O. P. Welzel, C. Harrison, X. F. Wang, X. H. Chen, F. M. Grosche, and P. G. Niklowitz, J. Phys. Condens. Matter **22**, 052201 (2010).
[24] M. Rotter, C. Hieke, and D. Johrendt, Phys. Rev. B **82**, 014513 (2010).
[25] D. Hu *et al.*, Phys. Rev. Lett. **114**, 157002 (2015).
[26] T. Shimojima *et al.*, Phys. Rev. B **89**, 045101 (2014).
[27] T. Sonobe *et al.*, Sci. Rep. **8**, 2169 (2018).
[28] S. Kasahara *et al.*, Nature (London) **486**, 382 (2012).
[29] L. Stojchevska, T. Mertelj, J.-H. Chu, I. R. Fisher, and D. Mihailovic, Phys. Rev. B **86**, 024519 (2012).
[30] M. Cardona, K. L. Shaklee, and F. H. Pollak, Phys. Rev. **154**, 696 (1967).
[31] N. Tamura, A. A. MacDowell, R. Spolenak, B. C. Valek, J. C. Bravman, W. L. Brown, R. S. Celestre, H. A. Padmore, B. W. Batterman, and J. R. Patel, J. Synchrotron Radiat. **10**, 137 (2003).
[32] K. W. Song and A. E. Koshelev, Phys. Rev. B **94**, 094509 (2016).
[33] See Supplemental Material at http://link.aps.org/supplemental/10.1103/PhysRevLett.121.027001 for, Sec. S1, for data on the fluence dependence of T_c.
[34] See Supplemental Material at http://link.aps.org/supplemental/10.1103/PhysRevLett.121.027001 for, Sec. S2, for a justification of the use of the antisymmetric component of the photomodulation response as a proxy for nematic order.
[35] See Supplemental Material at http://link.aps.org/supplemental/10.1103/PhysRevLett.121.027001 for, Sec. S3, for a description of the model of photomodulation response based on competing superconducting and nematic order parameters.
[36] M. A. Tanatar, A. Kreyssig, S. Nandi, N. Ni, S. L. Bud'ko, P. C. Canfield, A. I. Goldman, and R. Prozorov, Phys. Rev. B **79**, 180508 (2009).

[37] M. A. Tanatar *et al.*, Phys. Rev. B **81**, 184508 (2010).
[38] J.-H. Chu, J. G. Analytis, D. Press, K. De Greve, T. D. Ladd, Y. Yamamoto, and I. R. Fisher, Phys. Rev. B **81**, 214502 (2010).
[39] H.-H. Kuo, J. G. Analytis, J.-H. Chu, R. M. Fernandes, J. Schmalian, and I. R. Fisher, Phys. Rev. B **86**, 134507 (2012).
[40] A. E. Böhmer, A. Sapkota, A. Kreyssig, S. L. Bud'ko, G. Drachuck, S. M. Saunders, A. I. Goldman, and P. C. Canfield, Phys. Rev. Lett. **118**, 107002 (2017).
[41] See Supplemental Material at http://link.aps.org/supplemental/10.1103/PhysRevLett.121.027001 for, Sec. S4, for a description of the procedure used to align the optical and x-ray maps.
[42] See Supplemental Material at http://link.aps.org/supplemental/10.1103/PhysRevLett.121.027001 for, Sec. S5, for evidence that variations in strain anisotropy are not due to either the mounting or the cooling process.
[43] S. E. Brown, E. Fradkin, and S. A. Kivelson, Phys. Rev. B **71**, 224512 (2005).